Electronic Supplementary Information

Boosting Alkaline Water Splitting Efficiency: NiOOH-MnOOH Heterojunctions via In Situ Anodic Oxidation

Yuru Zhou[a], Jing Hu*[a], Yinan Liu[a], Wenyu Fan[a], Panpan Tao[a], Rui Yang[a], Haitao Huang[a], Xun Cao*[b], Haijin Li[a] and Siwei Li*[c]

[a] School of Energy and Environment, Anhui University of Technology, Ma'anshan, Anhui 243002, P. R. China

[b] Institute of Sustainability for Chemicals, Energy and Environment (ISCE2), Agency for Science, Technology and Research (A*STAR), 1 Pesek Road, Jurong Island, Singapore 627833, Singapore

[c] Institute of Industrial Catalysis, School of Chemical Engineering and Technology, Xi'an Jiaotong University, Xi'an, 710049 P. R. China

*Corresponding authors: E-mail: jennyhu@ahut.edu.cn (J.H.); Cao_Xun@isce2.a-star.edu.sg (X.C.); lisiwei@xjtu.edu.cn (S.L.)

Calibration of reference electrode

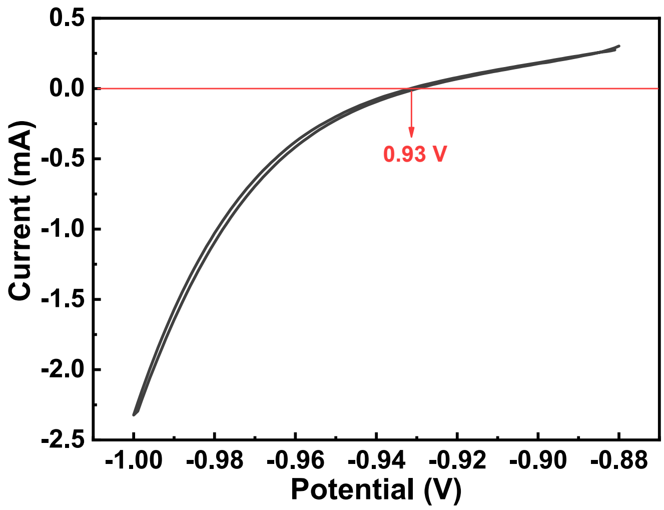

Fig. S1 The cyclic voltammetry (CV) curve of the calibration of Hg/HgO in 1.0 M KOH.

Calibration was carried out in 1.0 M KOH solution saturated with high purity hydrogen and the working electrode was a platinum foil. As the current approaches zero, the average of the two potentials (-0.93 V) is determined as the thermodynamic potential. Thus, $E_{(RHE)}$ can be calculated by the following equation: $E_{(RHE)} = E_{(Hg/HgO)} + 0.93$ V

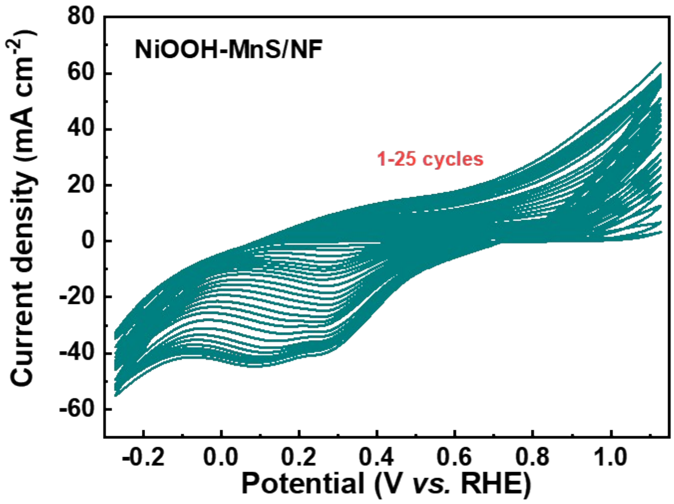

Fig. S2 Electrodeposition curve of NiOOH-MnOOH/NF sample.

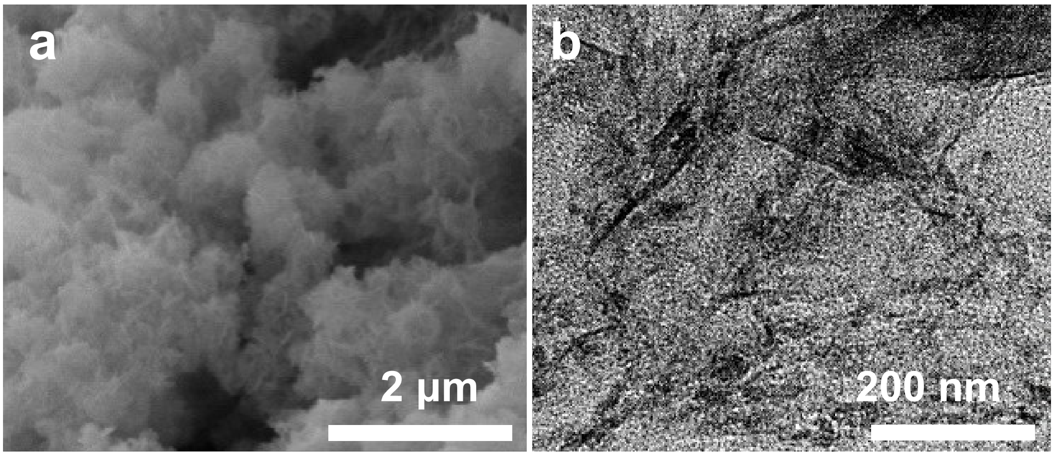

Fig. S3 (a) SEM image, (b) TEM image of Mn_3O_4/NF sample.

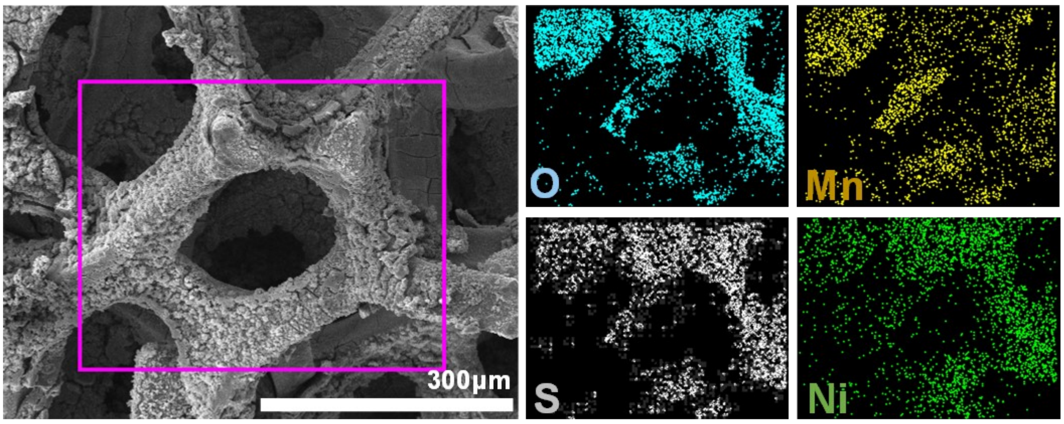

Fig. S4 Element mapping for vertically aligned NiOOH-MnS/NF.

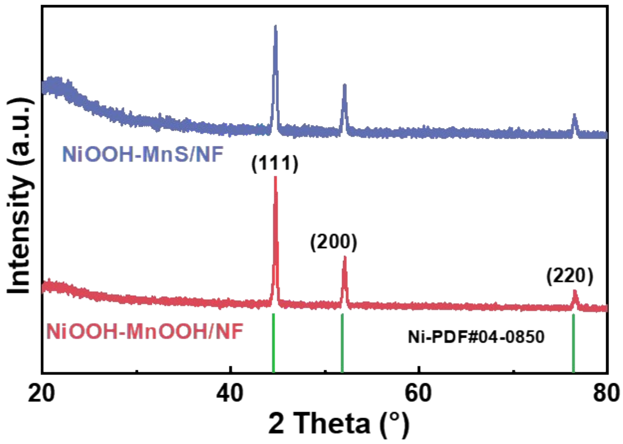

Fig. S5 The XRD patterns of NiOOH-MnS/NF and NiOOH-MnOOH/NF samples were measured directly on Ni foam.

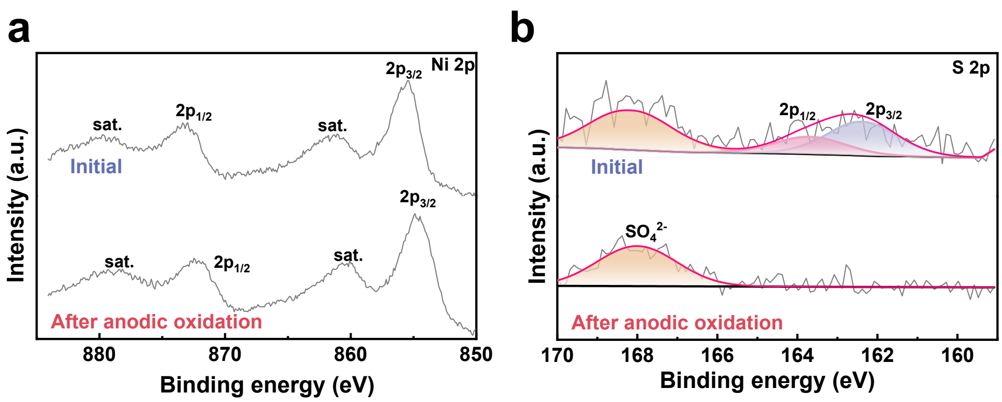

Fig. S6 (a) Ni 2p and (b) S 2p XPS spectra of electrocatalysts before and after the anodic oxidation process.

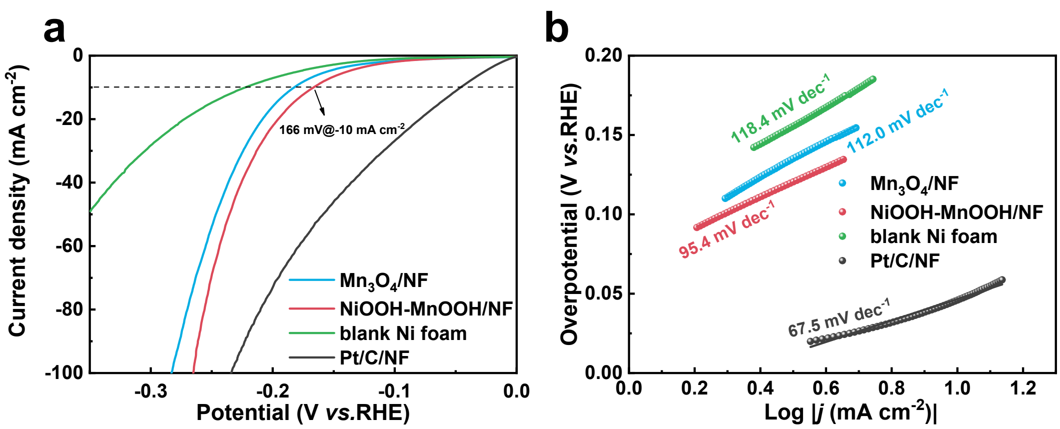

Fig. S7 (a) HER polarization curves of the prepared samples after *i*R correction. (b) Tafel plots.

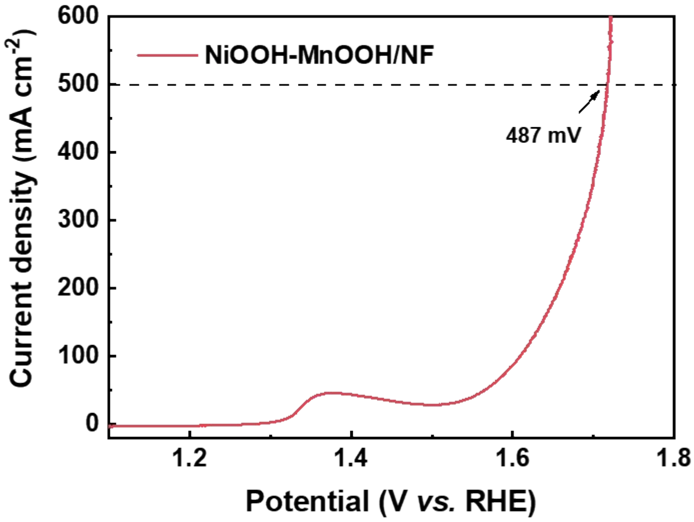

Fig. S8 LSV curve of the samples of NiOOH-MnOOH/NF after *i*R correction at 500 mA cm^{-2} in 1.0 M KOH.

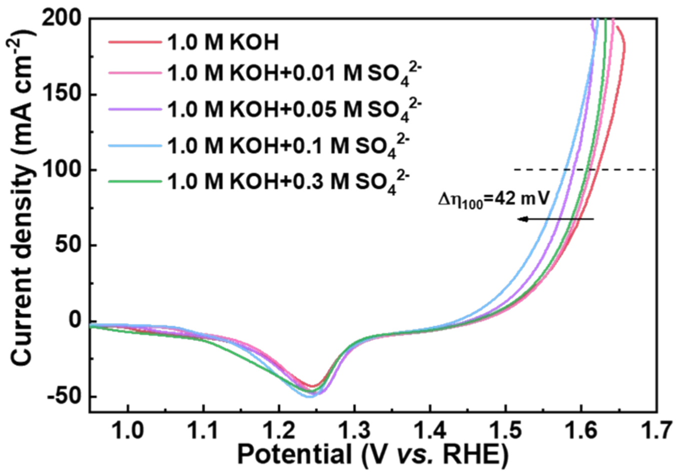

Fig. S9 LSV curves of the sample of NiOOH-MnOOH/NF after *i*R correction in 1.0 M KOH solution added with different concentrations of SO_4^{2-}.

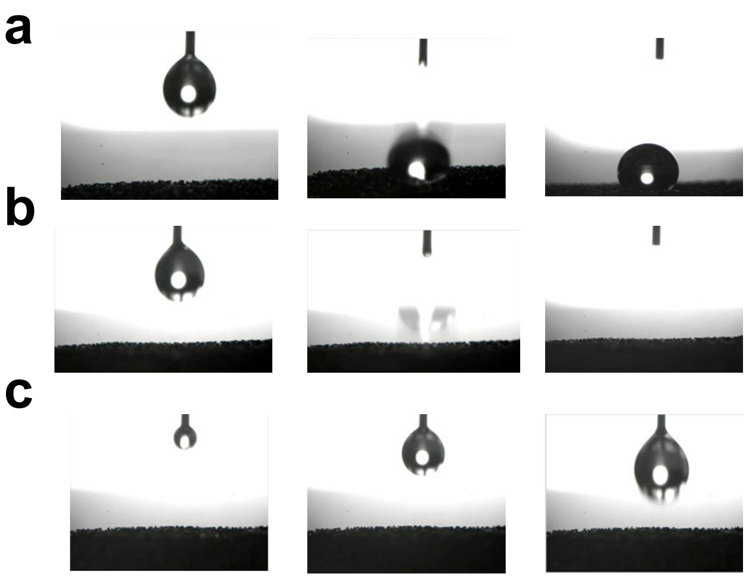

Fig. S10 Contact angle photographs of the droplet experiment of (a)blank Ni foam, (b) NiOOH-MnS/NF, (c) NiOOH-MnOOH/NF.

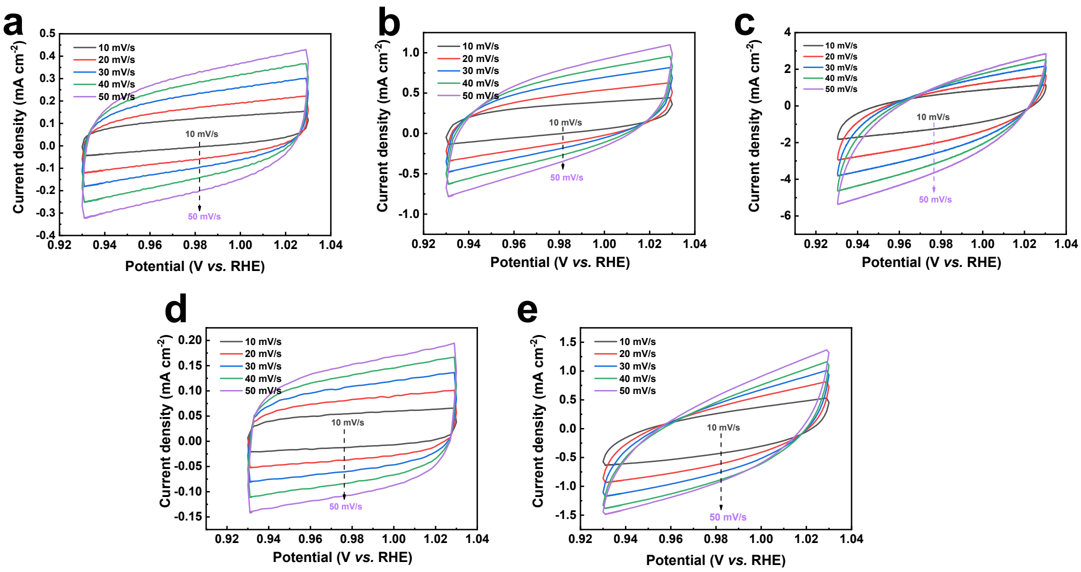

Fig. S11 CV curves of (a) Mn_3O_4/NF, (b) NiOOH-MnS/NF, (c) NiOOH-MnOOH/NF, (d) blank Ni foam and and (e) RuO_2/NF samples in 1.0 M KOH solution at different scan rates (10, 20, 30, 40 and 50 mV s^{-1}).

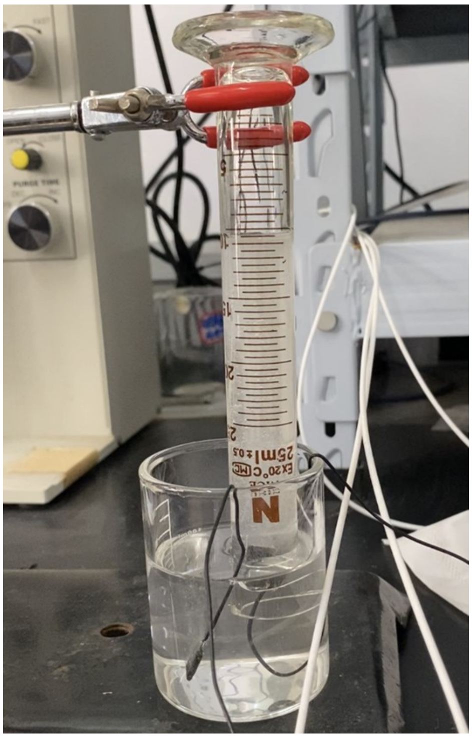

Fig. S12 Digital photographs of Faraday's efficiency.

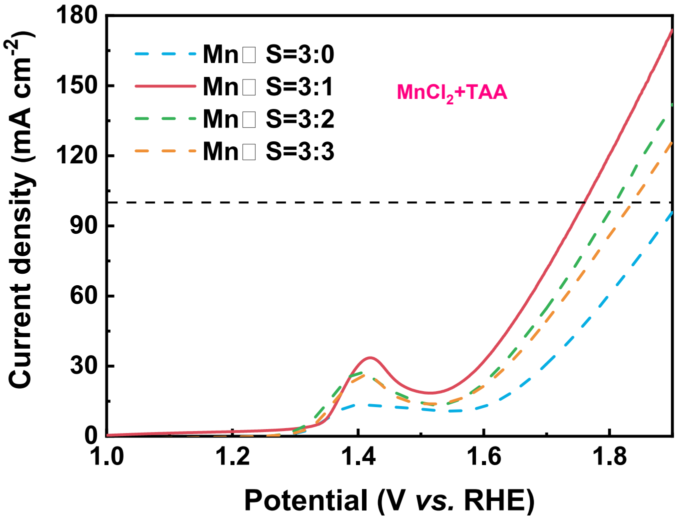

Fig. S13 LSV curves of different manganese-sulfur ratios.

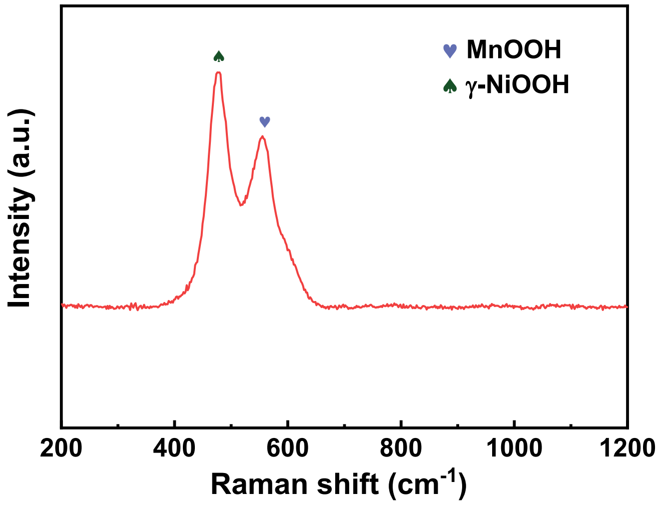

Fig. S14 Raman spectra of the samples of NiOOH-MnOOH/NF after 100 CV cycles.

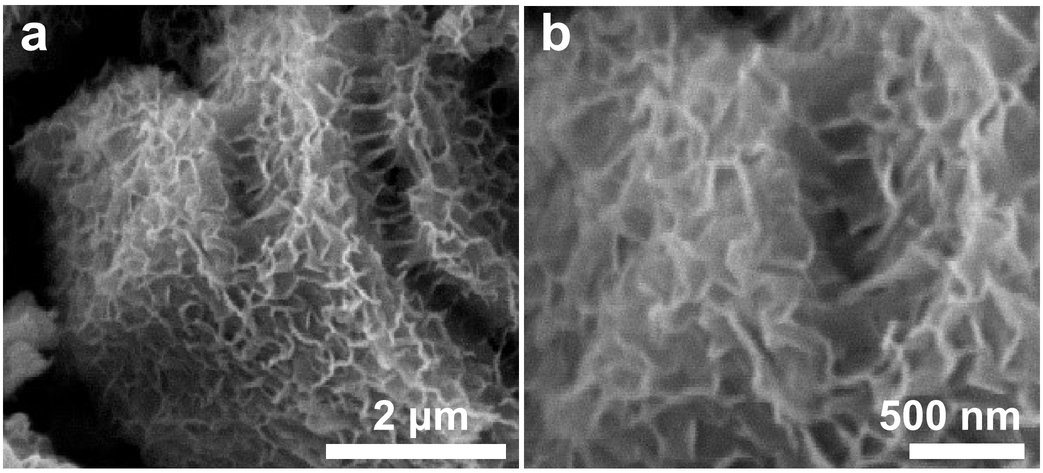

Fig. S15 SEM images of samples of NiOOH-MnOOH/NF after 100 CV cycles.

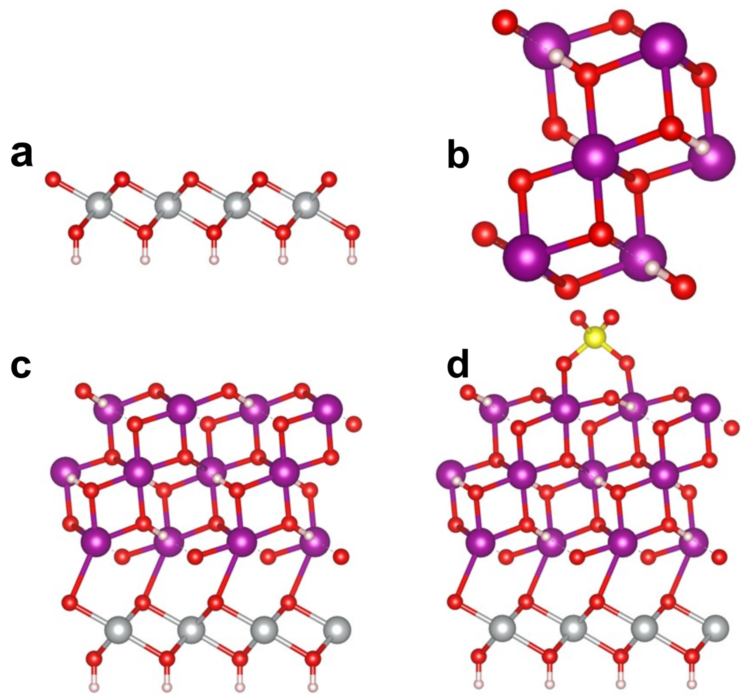

Fig. S16 Atomic model of (a) NiOOH, (b) MnOOH, (c) NiOOH-MnOOH, (d) NiOOH-MnOOH-SO_4^{2-}, The gray, purple, red, pink, and yellow balls represent Ni, Mn, O, H, and S atoms, respectively.

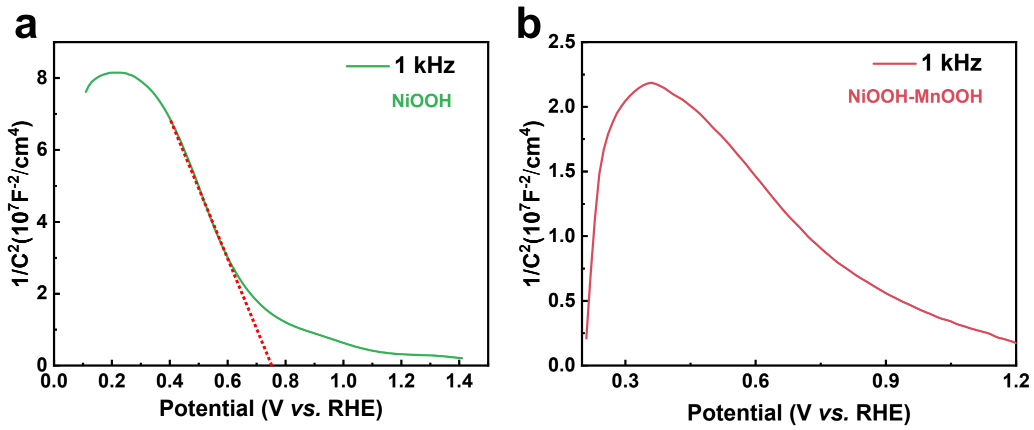

Fig. S17 Mott-Schottky curves of (a) NiOOH and (b) NiOOH-MnOOH. (The electrolyte is 0.5 M Na_2SO_4 solution)

The structural type of the catalyst was inquired by the Mott-Schottky (M-S) test to research the structure of the catalyst. Upon analysis of the tested M-S curves, it was shown that the negative slope of the curve for NiOOH corresponded to a p-type semiconductor. The M-S plot of NiOOH-MnOOH after anodic oxidation showed an inverted "V" shape with positive and negative slopes, indicating that a p-n interface was formed on the surface of the catalyst, which constituted a p-n heterostructure.[16]

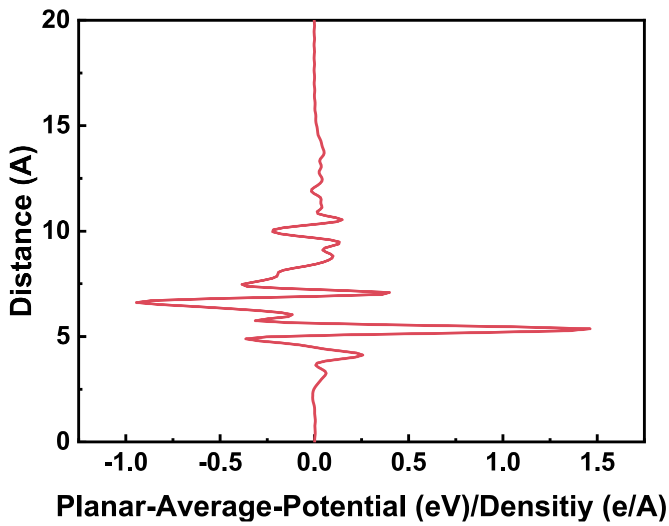

Fig. S18 Plane-averaged charge density difference Δρ(x) of NiOOH-MnOOH-SO_4^{2-} along the z direction normal to the surface.

Table S1-4:

Table S1. Comparison of the OER performance for NiOOH-MnOOH/NF with other related electrocatalysts.

Catalysts	η_{10} (mV)	η_{100} (mV)	Tafel slop (mV dec^{-1})	Ref
NiOOH-MnOOH/NF	**276**	**391**	**52.3**	**This work**
MnOOH@$CDs_{0.2}$	302		51.3	1
γ-MnOOH/NF	355		283	2
β-MnOOH/NF	395	543	87	3
Ni–MnO/rGO	370		67	4
NS-MnO_2	320		40	5
MnO_2-CoP_3	288		60	6
Ni^{2+}/MnO_2	400		72	7
Ni-MnS	349	450	87	8
CoMnNiS	371	440	48.2	9
Co/Co_9S_8/MnS-NMC	330	420	55.1	10
γ-MnOOH/CoOOH	313	390	87	11
CoMn LDH	350		43	12
MnO_2-NiO	379		47.8	13

$NiMnO_3/NiMn_2O_4$	380	73.3	[14]
$CoMn_2O_4$	310	93.5	[15]

Table S2. The free energy change (ΔG) of each elementary reaction for OER on different catalysts at U = 0 V.

Models	ΔG_1 (eV)	ΔG_2 (eV)	ΔG_3 (eV)	ΔG_4 (eV)
NiOOH	2.21	0.76	2.33	-0.38
MnOOH	0.33	1.26	2.07	1.27
NiOOH-MnOOH	0.03	1.25	1.86	1.79
NiOOH-MnOOH-SO_4^{2-}	0.22	1.68	1.27	1.75

Table S3. The free energy change (ΔG) of each elementary reaction for OER on different catalysts at U = 1.23 V.

Models	ΔG_1 (eV)	ΔG_2 (eV)	ΔG_3 (eV)	ΔG_4(eV)
NiOOH	0.98	-0.47	1.10	-1.61
MnOOH	-0.90	0.03	0.84	0.04
NiOOH-MnOOH	-1.20	0.02	0.63	0.56
NiOOH-MnOOH-SO_4^{2-}	-1.01	0.45	0.04	0.52

Table S4. Bader charges (in the unit e^-) for Mn and Ni atoms in the NiOOH, MnOOH, NiOOH-MnOOH, hetero-structured NiOOH-MnOOH-SO_4^{2-}

Bader charge	Ni	Mn
NiOOH	0	
MnOOH		0
NiOOH-MnOOH	0.051	-0.001
NiOOH-MnOOH-SO_4^{2-}	0.050	-0.035

Note: Setting the charges of Ni and Mn in pure NiOOH and MnOOH to 0 to compare the electron gains and losses after the formation of heterojunctions

References

1 L. Tian, X. Zhai, X. Wang, X. Pang, J. Li and Z. Li, Morphology and phase transformation of α-MnO_2/MnOOH modulated by N-CDs for efficient electrocatalytic oxygen evolution reaction in alkaline medium, *Electrochim. Acta*, 2020, **337**.

2 S.-B. Wang, Y.-S. Xia, Z.-F. Xin and L.-X. Xu, Fabrication of the novel NiFe-LDHs @γ-

MnOOH nanorod electrocatalyst for effective water oxidation, *Catal. Commun.*, 2023, **173**.

3 C. Walter, S. Kalra, R. Beltrán-Suito, M. Schwarze, P. W. Menezes and M. Driess, Manganese sulfide enables the formation of a highly active β-MnOOH electrocatalyst for effective alkaline water oxidation, *Mater. Today Chem.*, 2022, **24**.

4 G. Fu, X. Yan, Y. Chen, L. Xu, D. Sun, J. M. Lee and Y. Tang, Boosting bifunctional oxygen electrocatalysis with 3D graphene aerogel-supported Ni/MnO particles, *Adv. Mater.*, 2017, **30**.

5 Y. Zhao, C. Chang, F. Teng, Y. Zhao, G. Chen, R. Shi, G. I. N. Waterhouse, W. Huang and T. Zhang, Defect-engineered ultrathin δ-MnO_2 nanosheet arrays as bifunctional electrodes for efficient overall water splitting, *Adv. Energy Mater.*, 2017, **7**.

6 X. Xiong, Y. Ji, M. Xie, C. You, L. Yang, Z. Liu, A. M. Asiri and X. Sun, MnO_2-CoP_3 nanowires array: An efficient electrocatalyst for alkaline oxygen evolution reaction with enhanced activity, *Electrochem. Commun.*, 2018, **86**, 161-165.

7 A. C. Thenuwara, E. B. Cerkez, S. L. Shumlas, N. H. Attanayake, I. G. McKendry, L. Frazer, E. Borguet, Q. Kang, R. C. Remsing, M. L. Klein, M. J. Zdilla and D. R. Strongin, Nickel confined in the interlayer region of birnessite: an active electrocatalyst for water oxidation, *Angew. Chem. Int. Edit.*, 2016, **55**, 10381-10385.

8 G. A. Tigwere, M. D. Khan, L. D. Nyamen, F. M. de Souza, W. Lin, R. K. Gupta, N. Revaprasadu and P. T. Ndifon, Transition metal (Ni, Cu and Fe) doped MnS nanostructures: Effect of doping on supercapacitance and water splitting, *Mat. Sci. Semicon. Proc.*, 2023, **158**.

9 M. Verma, L. Sinha and P. M. Shirage, Electrodeposited nanostructured flakes of cobalt, manganese and nickel-based sulfide (CoMnNiS) for electrocatalytic alkaline oxygen evolution reaction (OER), *J. Mater. Sci-Mater. El.*, 2021, **32**, 12292-12307.

10 K. Chen, X. Wang, C. Zhang, R. Xu, H. Wang, L. Chu and M. Huang, Three-phases Co/Co_9S_8/MnS heterostructures engineering for boosted ORR/OER activities in Zn–air batteries, *Mater. Today Energy*, 2022, **30**.

11 M. Cui, H. Zhao, X. Dai, Y. Yang, X. Zhang, X. Luan, F. Nie, Z. Ren, Y. Dong, Y. Wang, J. Yang and X. Huang, Promotion of the electrocatalytic oxygen evolution reaction by chemical coupling of CoOOH particles to 3D branched γ-MnOOH rods, *Acs Sustain. Chem. Eng.*, 2019, **7**, 13015-13022.

12 F. Song and X. Hu, Ultrathin cobalt–manganeselayered double hydroxide is an efficient oxygen evolution catalyst, *J. Am. Chem. Soc.*, 2014, **136**, 16481-16484.

13 S. P. Mooni, K. K. Kondamareddy, S. Li, X. Zhou, L. Chang, X. Ke, X. Yang, D. Li and Q. Qu, Graphene oxide decorated bimetal (MnNi) oxide nanoflakes used as an electrocatalyst for enhanced oxygen evolution reaction in alkaline media, *Arab. J. Chem.*, 2020, **13**, 4553-4563.

14 X. He, F. Yin, Y. Li, H. Wang, J. Chen, Y. Wang and B. Chen, $NiMnO_3$/$NiMn_2O_4$ oxides synthesized via the aid of pollen: Ilmenite/Spinel hybrid nanoparticles for highly efficient bifunctional oxygen electrocatalysis, *Acs Appl. Mater. Inter.*, 2016, **8**, 26740-26757.

15 A. Bahadur, W. Hussain, S. Iqbal, F. Ullah, M. Shoaib, G. Liu and K. Feng, A morphology controlled surface sulfurized $CoMn_2O_4$ microspike electrocatalyst for

water splitting with excellent OER rate for binder-free electrocatalytic oxygen evolution, *J. Mater. Chem. A*, 2021, **9**, 12255-12264.
16 G. Fang, X. Ji, H. Shi, C. Zhang, Z. Guo, T. Tang and W. Liu, Constructing built-in electric field in 3D core-shell p-n heterostructure of NiFe-LDH nanosheets modified Cr-doped Ni_3S_2 nanofibers for efficient and stable oxygen evolution reaction, *J. Alloy. Compd.*, 2024, **970**, 172583.